Microarray Analysis of Iris Gene Expression in Mice with Mutations Influencing Pigmentation

Colleen M. Trantow,[1] *Tryphena L. Cuffy,*[2] *John H. Fingert,*[2,3] *Markus H. Kuehn,*[2,3] *and Michael G. Anderson*[1,2,3]

Purpose. Several ocular diseases involve the iris, notably including oculocutaneous albinism, pigment dispersion syndrome, and exfoliation syndrome. To screen for candidate genes that may contribute to the pathogenesis of these diseases, genome-wide iris gene expression patterns were comparatively analyzed from mouse models of these conditions.

Methods. Iris samples from albino mice with a *Tyr* mutation, pigment dispersion–prone mice with *Tyrp1* and *Gpnmb* mutations, and mice resembling exfoliation syndrome with a *Lyst* mutation were compared with samples from wild-type mice. All mice were strain (C57BL/6J), age (60 days old), and sex (female) matched. Microarrays were used to compare transcriptional profiles, and differentially expressed transcripts were described by functional annotation clustering using DAVID Bioinformatics Resources. Quantitative real-time PCR was performed to validate a subset of identified changes.

Results. Compared with wild-type C57BL/6J mice, each disease context exhibited a large number of statistically significant changes in gene expression, including 685 transcripts differentially expressed in albino irides, 403 in pigment dispersion–prone irides, and 460 in exfoliative-like irides.

Conclusions. Functional annotation clusterings were particularly striking among the overrepresented genes, with albino and pigment dispersion–prone irides both exhibiting overall evidence of crystallin-mediated stress responses. Exfoliative-like irides from mice with a *Lyst* mutation showed overall evidence of involvement of genes that influence immune system processes, lytic vacuoles, and lysosomes. These findings have several biologically relevant implications, particularly with respect to secondary forms of glaucoma, and represent a useful resource as a hypothesis-generating dataset. (*Invest Ophthalmol Vis Sci.* 2011;52:237–248) DOI:10.1167/iovs.10-5479

The iris plays an essential role in regulating the amount of light passing to the retina and is also important in many human diseases. Several diseases change iris pigmentation, including forms of oculocutaneous albinism, Hermansky-Pudlak syndrome, Chediak-Higashi syndrome, Horner's syndrome, Waardenburg syndrome, and Fuchs' heterochromic iridocyclitis. In addition, other ocular diseases, such as pigment dispersion syndrome and exfoliation syndrome, involve disease-related morphologic changes to the pigmented tissues of the iris. Each of these diseases involves strong hereditary links, but much remains unknown concerning the underlying genetic pathways. In this study, we focused on three of these conditions: albinism, pigment dispersion syndrome, and exfoliation syndrome.

In oculocutaneous albinism (OCA), there is reduced or absent pigmentation of the skin, hair, and eyes. Decreased melanin in the eyes can give rise to several ocular abnormalities, including foveal hypoplasia and decreased visual acuity; retinal ganglion cell axon misrouting; and strabismus, nystagmus, iris translucency, color vision impairment, and photophobia.[1] The hereditary basis of OCA is complex. There are at least 4 genes that contribute to classic forms of OCA and at least another 12 associated with syndromic forms. The best understood form of OCA, and the most common in many populations, is OCA1.[2,3] OCA1 is caused by mutations in the tyrosinase (*TYR*) gene, which encodes the rate-limiting enzyme necessary for melanin synthesis. Most people with OCA1 are believed to be compound heterozygotes, although in 15% of OCA1 cases, the second mutation remains unidentified.[4] Interestingly, TYR appears to also influence many traits beyond pigmentation. For example, tyrosinase mutation is capable of rescuing a mouse model of pigment dispersion,[5] but acts to worsen disease in mouse models of developmental glaucoma.[6] Clearly, much remains unknown concerning TYR and its influences on ocular disease.

In pigment dispersion syndrome, liberated pigment from the iris pigment epithelium becomes aberrantly deposited throughout the anterior chamber. As pigment accumulates in the iridocorneal angle, aqueous humor outflow resistance and intraocular pressure can become elevated.[7,8] Although pigment dispersion syndrome has strong hereditary links,[9,10] the genetic risk factors remain to be identified. DBA/2J mice develop a form of pigmentary glaucoma involving a pigment-dispersing iris disease, elevated intraocular pressure, and optic nerve damage.[11,12] Mutations in two genes encoding melanosomal proteins, *Tyrp1* and *Gpnmb*, are responsible for initiation of the DBA/2J disease process.[13] To date, genetic studies of *TYRP1* and *GPNMB* in human pigment dispersion patients have not detected mutations,[13,14] suggesting that other genes in a pathway linked to *TYRP1* and *GPNMB* may be the next most logical candidates worthy of consideration.

In exfoliation syndrome, a primary diagnostic feature is the presence of fibrillar exfoliative material throughout the anterior chamber of the eye.[15] The disease often also involves the dispersion of iris pigment and morphologic changes to the structure of the iris pigment epithelium.[16,17] As with pigment dispersion syndrome, accumulations of material within the iridocorneal angle can obstruct aqueous humor outflow, result-

From the [1]Department of Molecular Physiology and Biophysics, the [2]Interdisciplinary Graduate Program in Genetics, and the [3]Department of Ophthalmology and Visual Sciences, University of Iowa, Iowa City, Iowa.

Supported by National Eye Institute Grant EY017673 and Supplementary Grant EY017673-0282 (MGA) and a Grant from The Glaucoma Foundation (MGA, JHF). MHK is supported by National Eye Institute Grant EY019485.

Submitted for publication March 5, 2010; revised July 27, 2010; accepted August 8, 2010.

Disclosure: **C.M. Trantow**, None; **T.L. Cuffy**, None; **J.H. Fingert**, None; **M.H. Kuehn**, None; **M.G. Anderson**, None

Corresponding author: Michael G. Anderson, Department of Molecular Physiology and Biophysics, 6-430 Bowen Science Building, 51 Newton Road, Iowa City, IA 52242; michael-g-anderson@uiowa.edu.

Copyright 2011 The Association for Research in Vision and Ophthalmology, Inc.

ing in elevated intraocular pressure and glaucoma. Recently, genetic variations in the *LOXL1* gene have been linked with exfoliation syndrome.[18] Because the same *LOXL1* alleles associated with exfoliation syndrome also occur in the general population at a very high frequency, additional risk factors are presumed to exist. B6-*Lyst*$^{bg\text{-}J}$ mice exhibit multiple ocular features resembling exfoliation syndrome, including the presence of an exfoliative-like material, pigment dispersion, and iris transillumination defects caused by an apparent loss of cell–cell adhesions within the iris pigment epithelium.[17] Accordingly, *LYST* and other genes within the *LYST* genetic pathway are candidates that are likely to contribute to exfoliation syndrome in humans.

We report global gene expression patterns of the iris in four strains of mice with identical genetic backgrounds: wild-type C57BL/6J mice with normal irides, albino mice with *Tyr* mutation, pigment dispersion–prone mice with *Tyrp1* and *Gpnmb* mutations, and exfoliative-like mice with *Lyst* mutation. In each comparison between these strains, transcriptional changes are presented for select genes of functionally annotated clusters and are also presented according to the magnitude of the ratio of change.

METHODS

Animal Husbandry

Wild-type C57BL/6J, albino B6(Cg)-*Tyr*$^{c\text{-}2J}$/J (abbreviated throughout as B6.*Tyr*$^{c\text{-}2J}$), and exfoliative-like B6-*Lyst*$^{bg\text{-}J}$/J (abbreviated throughout as B6-*Lyst*$^{bg\text{-}J}$) mice were commercially obtained from The Jackson Laboratory (Bar Harbor, ME). A pigment dispersion–prone, double-congenic stock homozygous for congenic intervals containing the pigment dispersion–causing *Tyrp1*^{b} and *Gpnmb*^{R150X} mutations on the B6 genetic background (B6.D2-*Tyrp1*^{b}*Gpnmb*^{R150X}/Sj, in this study, after abbreviated B6.*Tyrp1*^{b} *Gpnmb*^{R150X})[5] was initially obtained from Simon John (The Jackson Laboratory) and subsequently bred at the University of Iowa. All mice were female, and all experiments with mutant mice used mice homozygous for the respective mutations. The mice were housed at the University of Iowa Research Animal Facility, maintained on a 4% fat NIH 31 diet provided ad libitum, and housed in cages containing dry bedding (Cellu-dri; Shepherd Specialty Papers, Kalamazoo, MI). The environment was kept at 21°C with a 12-hour light:12-hour dark cycle. All animals were treated in accordance with the ARVO Statement for the Use of Animals in Ophthalmic and Vision Research. All experimental protocols were approved by the Animal Care and Use Committee of The University of Iowa.

Mouse Slit Lamp Examination

Anterior chamber phenotypes were assayed with a slit lamp biomicroscope (SL-D7; Topcon, Tokyo, Japan) and photodocumented with a digital camera (D100; Nikon, Tokyo, Japan). For assessment of anterior chamber phenotypes with broad-beam illumination, a beam of light was shone at an angle across the eye, and the anterior chamber was examined. For assessment of iris transillumination defects, a small beam of light was shone directly through the undilated pupil of the mouse, and the iris was examined for the ability of reflected light to pass through diseased or depigmented areas of the iris. All ocular examinations were performed in conscious mice. All photographs were taken with identical camera settings and prepared with identical image software processing. Slit lamp and iris phenotypes have been reported for all the strains used, including C57BL/6J,[19,20] B6.*Tyr*$^{c\text{-}2J}$,[5,19–20] B6.*Tyrp1*^{b} *Gpnmb*^{R150X},[5] and B6-*Lyst*$^{bg\text{-}J}$[17,19,20] and are also shown in Figures 1 and 2.

Microarray Analysis

Gene expression profiling was performed on irides from 60-day-old female C57BL/6J, B6.*Tyr*$^{c\text{-}2J}$, B6.*Tyrp1*^{b} *Gpnmb*^{R150X}, and B6-*Lyst*$^{bg\text{-}J}$ mice. Enucleated eyes were dissected in phosphate-buffered saline with both irides from each mouse pooled to form one sample; three samples (mice) were analyzed per strain. Iris samples were homogenized, and RNA was extracted, treated with DNase I, and purified (Aurum Total RNA Mini Kit; Bio-Rad Laboratories; Hercules, CA). RNA was subsequently purified by EtOH precipitation and quantified (Quant-iT RiboGreen RNA Assay Kit; Molecular Probes, Eugene, OR) and the integrity confirmed on a bioanalyzer (model 2100; Agilent Technologies, Inc., Palo Alto, CA). RNA samples were converted to cRNA compatible with gene microarrays according to the manufacturer's standard protocols and hybridized (Mouse Genome 2.0 arrays; Affymetrix, Santa Clara, CA). Raw data were normalized by using the RMA (robust multichip average) algorithm, and quality was assessed with PLM (probe level model) methodology.[21] Normalized data were $\log_2$ transformed and filtered to remove probesets that did not display expression levels above 5.0 in at least two samples and those that did not display at least a 1.8-fold difference between the highest and lowest expression values. The remaining probesets were then evaluated using the significance analysis for microarray algorithm to identify significant expression changes (SAM; ver. 3.05; Excel Add-In; Microsoft, Redmond, WA).[22] Significance was determined by using a two-class, unpaired Wilcoxon rank sum test with 100 permutations. In the comparison of C57BL/6J versus B6.*Tyr*$^{c\text{-}2J}$, the delta value was 0.373, resulting in the identification of 4304 probesets with an estimated false discovery rate (FDR) of 3.7%. In the comparison of C57BL/6J versus B6.*Tyrp1*^{b} *Gpnmb*^{R150X}, the delta value was 0.329, resulting in the identification of 2893 probesets with an estimated FDR of 3.0%. In the comparison of C57BL/6J versus B6-*Lyst*$^{bg\text{-}J}$, the delta value was 0.339, resulting in the identification of 2633 probesets with an estimated FDR of 3.3%.

Probesets were subsequently linked to annotated genes and ordered. The number of genes expressed in C57BL/6J irides was estimated by linking probes with $\log_2$-transformed expression levels above 5.0 in at least two samples to gene annotations with a file provided by the microarray manufacturer (Mouse430_2.na28.annot; Affymetrix), eliminating duplicates of the same gene and eliminating unannotated probes. Lists of genes with changing expression were filtered (Excel; Microsoft) to include only probesets with at least a 1.8-fold change in expression. The probesets were first linked to annotated genes (Mouse430_2.na28.annot file). The remaining unlinked probesets were secondarily assigned to annotated genes by using the Gene List Report function from DAVID Bioinformatics Resources.[23,24] A small number of probesets could not be linked with any annotated genes and were removed from further analysis. In addition, one probeset (1436240_at) initially detected as having a >50-fold reduction in B6.*Tyrp1*^{b} *Gpnmb*^{R150X} irides was removed from the analysis. Although 1436240_at apparently links to the annotated gene *Tra2a* (which is immediately adjacent to *Gpnmb* on mouse chromosome 6), it appears to map to intronic DNA. Thus, it was unclear what gene this probe is actually reporting. Lists of annotated genes were subsequently filtered (Excel; Microsoft) to remove duplicates of the same gene, in which cases of only the largest ratio of change in expression is reported. This filtering yielded 685 unique annotated genes changing in the C57BL/6J versus B6.*Tyr*$^{c\text{-}2J}$ comparison, 403 genes changing in the C57BL/6J versus B6.*Tyrp1*^{b} *Gpnmb*^{R150X} comparison, and 460 genes changing in the C57BL/6J versus B6-*Lyst*$^{bg\text{-}J}$ comparison.

Functional annotation clustering was performed using DAVID Bioinformatics Resources.[23,24] Based on this ontology-based categorization, select clusters and associated genes were manually chosen for presentation in the tables. Eight clusters are presented for each comparison, including four that are shown for each comparison (pigmentation, immune system response, cell death, and neurodegeneration) and four that are representative and therefore may differ between comparisons. The complete data sets have been deposited in the National Center for Biotechnology Information's Gene Expression Omnibus under accession number GSE16994 (http://www.ncbi.nlm.nih.gov/ projects/geo/ provided by NCBI, National Institutes of Health, Bethesda, MD).

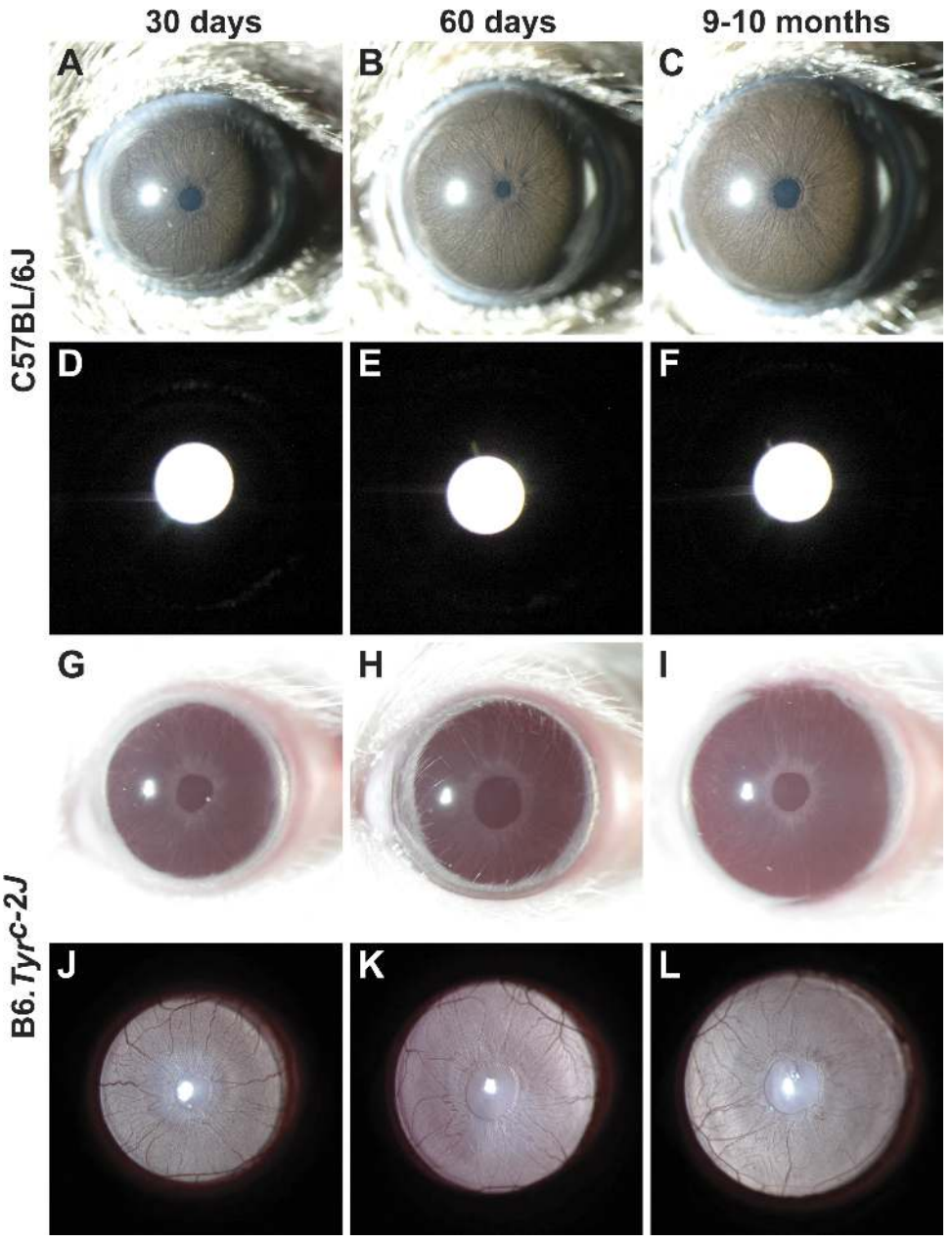

FIGURE 1. Iris phenotypes of wild-type C57BL/6J and albino B6.*Tyr*$^{c\text{-}2J}$ mice. Slit lamp images of eyes with broad-beam (*rows 1*, *3*) and transilluminating (*rows 2*, *4*) light. (**A–C**) At all ages, wild-type C57BL/6J irides had a smooth-appearing surface accentuated by numerous underlying vessels and a uniformly deep sienna-brown color. (**D–F**) With transilluminating illumination, C57BL/6J irides appeared black at all ages, indicating an intact healthy iris (the bright white circle is a reflection of the photographic flash and not an iris defect). (**G–I**) At all ages, B6.*Tyr*$^{c\text{-}2J}$ irides had a complete lack of melanin pigment, but otherwise remained intact. (**J–L**) With transilluminating illumination, B6.*Tyr*$^{c\text{-}2J}$ irides freely passed light across most areas. Because it is not transparent, the iridial vasculature was prominently visible.

Quantitative Real-Time PCR

To perform quantitative real-time PCR (qRT-PCR) analysis, we dissected the enucleated eyes in phosphate-buffered saline, and the irides from each mouse were pooled to form one sample; two samples (mice) were analyzed per strain. Iris samples were homogenized, RNA was extracted, treated with DNase I, purified (Aurum Total RNA Mini Kit; Bio-Rad Laboratories), and converted to cDNA (iScript cDNA Synthesis Kit; Bio-Rad Laboratories). Quantitative PCR was performed with a SYBR green mastermix (iQ SYBR Green Supermix; Bio-Rad Laboratories) in a real-time PCR detection system (iCycler MyiQ; Bio-Rad Laboratories). Each reaction contained: 2.5 μL water, 7.5 μL 2× iQ SYBR green mastermix, 2 μL 5′-primer (0.94 μM), 2 μL 3′-primer (0.94 μM), and 1 μL cDNA (1 ng/μL). Sequences for primer pairs used in the PCR reactions are available on request. PCR conditions were: 95°C for 3 minutes, 40× (95°C for 30 seconds, 60°C for 45 seconds). PCR products were subjected to melting curve analysis to ensure that only a single product was amplified. Each experiment included three technical replicates of each RNA sample. Expression data were quantified based on threshold cycle (C_t) values. For each transcript, C_t values for each sample were averaged and normalized to values of β-actin. Change analysis was based on $\Delta\Delta C_t$ and amplification efficiency of the transcripts.[25]

RESULTS

To screen for candidate genes that may contribute to the pathogenesis of OCA, pigment dispersion syndrome, and exfoliation syndrome, we used independent mouse models of these conditions on the C57BL/6J genetic background (Figs. 1, 2). All mice were also matched for age (60 days old) and sex (female). The rationale for this design was based on promoting homogeneity, because the iris phenotypes within each strain are indistinguishable between individual mice according to these criteria, the carefully matched animal cohorts should empower statistical significance in subsequent gene expression analysis.

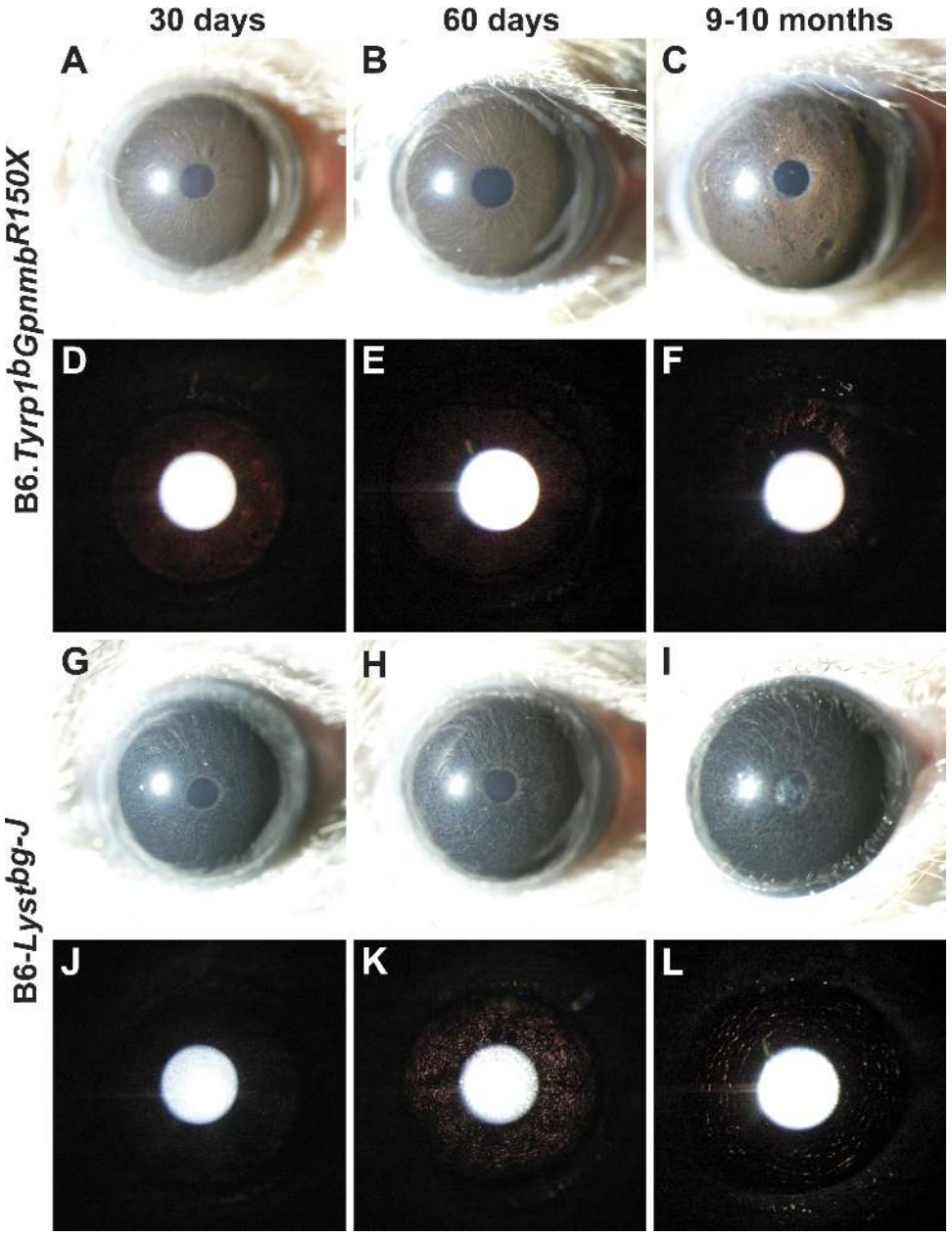

FIGURE 2. Iris phenotypes of pigment dispersion–prone B6.*Tyrp1*^{b} *Gpnmb*^{R150X} and exfoliative-like B6-*Lyst*$^{bg\text{-}J}$ mice. Slit lamp images of eyes with broad beam (*rows 1*, *3*) and transilluminating (*rows 2*, *4*) light. (**A**, **B**) Through 5 months of age, the irides of B6.*Tyrp1*^{b} *Gpnmb*^{R150X} mice were very similar to wild-type. (**C**) With increasing age, the pigment-dispersing iris disease in B6.*Tyrp1*^{b} *Gpnmb*^{R150X} mice was evident by the presence of dispersed pigment across the iris, giving it a granular appearance, and within the pupil. (**D**, **E**) With transilluminating light, B6.*Tyrp1*^{b} *Gpnmb*^{R150X} irides from young mice showed mild transillumination defects (*red areas*). (**F**) With increasing age, the transillumination defects of B6.*Tyrp1*^{b} *Gpnmb*^{R150X} mice became more apparent as iris atrophy accompanied pigment dispersion. (**G–I**) As a consequence of an early-onset degenerative disease, the iris of B6-*Lyst*$^{bg\text{-}J}$ mice appeared dark and granular. As observable in (**I**), cataracts were also common in B6-*Lyst*$^{bg\text{-}J}$ eyes. (**J–L**) With transilluminating light, B6-*Lyst*$^{bg\text{-}J}$ irides exhibited a distinct pattern of transillumination defects occurring in exfoliation syndrome characterized by concentric rings of transillumination.

C57BL/6J is a widely used inbred strain of mice with healthy irides lacking overt disease through advanced age.[19] Thus, at 60 days of age, the C57BL/6J iris is in a state of relative stasis, appearing uniformly deep sienna-brown in color and lacking transillumination defects (Figs. 1A–F). A large number of annotated genes (n = 18,234) were expressed in the iris of 60-day-old C57BL/6J mice. With expression levels in C57BL/6J irides used as the baseline, comparisons between C57BL/6J irides and each disease context detected many differences. Summaries of the data are presented according to the largest ratios of change (Table 1), the most significant gene ontology terms (Table 2), and manually selected examples of gene groupings associated with each comparison (Tables 3–8).

Transcriptional Differences between Albino and Pigmented Wild-Type Irides

Tyrosinase is the rate-limiting enzyme of melanin production.[4] The *Tyr*$^{c\text{-}2J}$ allele is a spontaneously arising missense mutation that also influences splicing of the tyrosinase pre-mRNA, ultimately resulting in complete absence of the tyrosinase protein.[26] The appearance of the B6.*Tyr*$^{c\text{-}2J}$ iris remains very consistent through advanced age.[5] Thus, at 60 days of age, the *Tyr*$^{c\text{-}2J}$ iris is in a state of relative stasis, primarily characterized by a complete absence of melanin pigment (Figs. 1G–L). To identify transcriptional differences related to tyrosinase-mediated absence or presence of melanin pigment production, microarray analysis was performed on RNA isolated from the iris of 60-day-old B6.*Tyr*$^{c\text{-}2J}$ mice.

The pair-wise comparison of RMA-normalized expression values between C57BL/6J and B6.*Tyr*$^{c\text{-}2J}$ irides identified 685 transcripts with >1.8-fold changes in expression (537 overrepresented and 148 underrepresented). Among the transcripts with the largest change ratio in expression (Table 1), the most striking observation was that several transcripts overrepresented in albino irides encoded crystallins (4 of the top 10; 10 of the top 25, data not shown). The most overrepresented transcripts were *Gja3* (+22.7-fold), *Mip* (+16.8-fold), and *B3gnt5* (+16.3-fold). The most underrepresented transcripts

TABLE 1. Top Gene Expression Changes

Overrepresented B6.*Tyr*$^{c\text{-}2J}$			Underrepresented B6.*Tyr*$^{c\text{-}2J}$		
Gene Symbol	**Gene Name**	**Change Ratio**	**Gene Symbol**	**Gene Name**	**Change Ratio**
Gja3	Gap junction membrane channel protein alpha 3	22.7	*Muc4*	Mucin 4	−5.2
Mip	Major intrinsic protein of eye lens fiber	16.8	*Myom2*	Myomesin 2	−4.3
B3gnt5	Udp-glcnac:betagal beta-1,3-n-acetylglucosaminyltransferase 5	16.3	*Cd274*	Cd274 antigen	−3.7
Cryba4	Crystallin, beta a4	13.7	*Ing3*	Inhibitor of growth family, member 3	−3.3
Cryba2	Crystallin, beta a2	11.9	*Mpzl2*	Myelin protein zero-like 2	−3.3
Cryga	Crystallin, gamma a	11.7	*Cck*	Cholecystokinin	−3.2
Cd24a	Cd24a antigen	11.0	*Scin*	Scinderin	−3.1
Crygb	Crystallin, gamma b	10.8	*Bhmt2*	Betaine-homocysteine methyltransferase 2	−3.1
Sox2ot	SOX2 overlapping transcript	10.3	*Slc6a6*	Solute carrier family 6, member 6	−3.0
Tmem40	Transmembrane protein 40	9.6	*Gm15698*	Predicted gene 15698	−3.0
Overrepresented B6.*Tyrp1*^{b} *Gpnmb*^{R150X}			**Underrepresented B6.*Tyrp1*^{b} *Gpnmb*^{R150X}**		
Gene Symbol	**Gene Name**	**Change Ratio**	**Gene Symbol**	**Gene Name**	**Change Ratio**
Gja3	Gap junction membrane channel protein alpha 3	12.4	*Gpnmb*	Glycoprotein (transmembrane) nmb	−9.4
B3gnt5	Udp-glcnac:betagal beta-1,3-n-acetylglucosaminyltransferase 5	9.2	*A230006I23RIK*	Riken cDNA A230006I23 gene	−8.5
Cryba2	Crystallin, beta a2	7.7	*Mysm1*	Myb-like, SWIRM and MPN domains 1	−3.5
Cryba4	Crystallin, beta a4	7.6	*Pisd-ps3*	Phosphatidylserine decarboxylase, pseudogene 3	−3.4
Sox2ot	SOX2 overlapping transcript	7.2	*Ing3*	Inhibitor of growth family, member 3	−3.3
Npl	N-acetylneuraminate pyruvate lyase	6.4	*Slc6a6*	Solute carrier family 6, member 6	−3.3
Cd24a	Cd24a antigen	6.3	*Prpmp5*	Proline-rich protein MP5	−3.2
Crybb3	Crystallin, beta b3	6.3	*Trpm1*	Transient receptor potential cation channel, subfamily m, member 1	−3.2
Grifin	Galectin-related inter-fiber protein	6.0	*C76798*	Expressed sequence C76798	−2.9
Crygb	Crystallin, gamma b	6.0	*Rapgef3*	Rap guanine nucleotide exchange factor (gef) 3	−2.9
Overrepresented B6.*Lyst*$^{bg\text{-}J}$			**Underrepresented B6.*Lyst*$^{bg\text{-}J}$**		
Gene Symbol	**Gene Name**	**Change Ratio**	**Gene Symbol**	**Gene Name**	**Change Ratio**
Mmp12	Matrix metallopeptidase 12	56.8	*Prpmp5*	Proline-rich protein MP5	−8.7
Fabp4	Fatty acid binding protein 4, adipocyte	44.4	*Krt12*	Keratin complex 1, acidic, gene 12	−6.1
Atp6v0d2	ATPase, H+ transporting, lysosomal V0 subunit D2	43.2	*Tmprss11e*	Transmembrane protease, serine 11E	−4.0
Il7r	Interleukin 7 receptor	31.3	*Krt6b*	Keratin complex 2, basic, gene 6B	−3.9
Clec4d	C-type lectin domain family 4, member D	30.1	*Krt5*	Keratin 5	−3.8
Cd36	CD36 antigen	25.0	*Krt6a*	Keratin complex 2, basic, gene 6A	−3.7
Itgb2	Integrin beta 2	20.0	*Dsp*	Desmoplakin	−3.7
Itgax	Integrin alpha x	16.6	*Slc22a8*	Solute carrier family 22, member 8	−3.5
Glipr1	Gli pathogenesis-related 1 (glioma)	16.3	*Muc4*	Mucin 4	−3.3
Clec7a	C-type lectin domain family 7, member A	15.5	*Ltbp2*	Latent transforming growth factor beta binding protein 2	−3.1

All changes relative to irides of age- and sex-matched C57BL/6J mice.

were *Muc4* (−5.2-fold), *Myom2* (−4.3-fold), and *Cd274* (−3.7-fold). Albino irides also exhibited expression changes in several groups of genes of biological interest (Tables 3, 4), including overrepresentation of several genes associated with visual perception and sensory organ development. Changes in transcripts prominently associated with pigmentation (such as *Oca2*, *Tyrp1*, *Matp*, *Dct*, and *Mc1r*) were not observed, nor were changes in expression of *Tyr* itself. Transcript levels of *Gpnmb*, which is associated with a pigment-dispersing iris disease dependent on tyrosinase function,[5,13] were underrepresented in albino irides (−2.1-fold).

Transcriptional Differences between Pigment Dispersion–Prone and Wild-Type Irides

The B6.*Tyrp1*^{b} *Gpnmb*^{R150X} strain is a double-congenic strain containing the pigment dispersion–causing *Tyrp1*^{b} and *Gpnmb*^{R150X} mutations on a C57BL/6J genetic background.[5] Thus, the strain contains the disease-causing mutations of the DBA/2J model of glaucoma,[13] but within a more widely used genetic background. *Tyrp1* encodes a transmembrane melanosomal protein with enzymatic activity required for melanogenesis. Compared with the wild-type C57BL/6J allele, the *Tyrp1*^{b}

TABLE 2. Top Gene Ontology Terms Identified by Analysis with DAVID Bioinformatics Resources

Mouse Strain	Gene Ontology Term	Genes	Benjamini Value
Overrepresented B6.*Tyr$^{c\text{-}2J}$*	Sensory perception of light stimulus	35	1.5E-23
	Visual perception	35	2.1E-23
	Structural constituent of eye lens	19	7.2E-20
	Sensory organ development	31	3.3E-12
Underrepresented B6.*Tyr$^{c\text{-}2J}$*	Protein modification process	26	5.0E-01
	Post-translational protein modification	23	6.3E-01
	Biopolymer modification	27	6.4E-01
	Purine ribonucleotide binding	25	9.5E-01
Overrepresented B6.*Tyrp1^{b} Gpnmb^{R150X}*	Structural constituent of eye lens	14	9.8E-15
	Anatomical structure development	67	2.2E-07
	Structural molecule activity	33	2.6E-07
Underrepresented B6.*Tyrp1*^{b} *Gpnmb^{R150X}*	Sensory organ development	19	5.0E-07
	Regulation of cellular process	29	9.8E-01
	Intracellular	54	6.0E-01
	Cytoplasm	38	7.6E-01
	Muscle development	6	1.0E+00
Overrepresented B6-*Lyst$^{bg\text{-}J}$*	Lysosome	18	1.7E-07
	Lytic vacuole	18	1.7E-07
	Immune system process	39	3.5E-07
	External side of plasma membrane	16	6.9E-07
Underrepresented B6-*Lyst$^{bg\text{-}J}$*	Ion transport	22	1.5E-02
	Extracellular matrix	14	1.6E-03
	Proteinaceous extracellular matrix	14	2.3E-03
	Anion transmembrane transporter activity	9	3.4E-02

Genes within individual gene ontology groups are not necessarily unique.

allele contains two missense mutations.[27] *Gpnmb* is predicted to also encode a transmembrane melanosomal protein, but its function is largely unknown.[13] Presumably a consequence of nonsense-mediated decay, the *Gpnmb^{R150X}* mutation has been shown to result in severely reduced *Gpnmb* transcript levels.[28] Through 5 months of age, the iris of B6.*Tyrp1^{b} Gpnmb^{R150X}* mice closely resembles wild-type.[5] From 6 to 18 months of age, the iris of B6.*Tyrp1^{b} Gpnmb^{R150X}* mice undergoes a pigment-dispersing iris disease that is very similar in severity and timing as in DBA/2J mice that are mutant for the same *Tyrp1* and *Gpnmb* alleles.[5,12,29] This iris disease ultimately involves pathologic contributions from both pigment-producing and bone-marrow–derived cells of the iris.[5,13,28,30] Thus, at 60 days of age, the B6.*Tyrp1^{b} Gpnmb^{R150X}* iris is in a pre to early stage of disease characterized by a normal appearing iris (Figs. 2A–F). To identify transcriptional differences related to pigment dispersion, microarray analysis was performed on RNA isolated from the iris of 60-day-old B6.*Tyrp1^{b} Gpnmb^{R150X}* mice.

The pair-wise comparison of RMA normalized expression values between C57BL/6J and B6.*Tyrp1^{b} Gpnmb^{R150X}* irides identified 403 transcripts with >1.8-fold changes in expression (300 overrepresented and 103 underrepresented). Among transcripts with the largest change in expression (Table 1), the most striking observation was that the signature of transcripts overrepresented in pigment dispersion–prone irides was very similar to the transcripts overrepresented in albino irides. Seven of the top 10 overrepresented transcripts observed in pigment dispersion–prone irides were also observed in the top 10 overrepresented transcripts of albino irides. Ten of the top 25 most overrepresented transcripts in pigment dispersion–prone irides encoded crystallins (data not shown). The most overrepresented genes were *Gja3* (+12.4-fold), *B3gnt5* (+9.2-fold), and *Cryba2* (+7.7-fold). As expected from previous work,[28] *Gpnmb* was underrepresented (−9.4-fold). *A230006123Rik* (−8.5-fold) and *Mysm* (−3.5-fold) were also among the most underrepresented transcripts. Pigment dispersion–prone irides exhibited expression changes in several groups of genes of biological interest (Tables 5, 6), including changes in the expression of several genes suspected of influencing glaucoma (*C1qb*, *Cntf*, and *Bcl2*).[31–33] Changes in *Tyrp1* expression were not detected.

Transcriptional Differences between Exfoliative-like and Wild-Type Irides

Lyst encodes a large cytosolic protein influencing lysosome-related organelles, including lysosomes, melanosomes, and platelet dense bodies.[34] Multiple mutant alleles of the *Lyst* gene have been identified in mice, including the *bg-J* mutation which results from a 3-bp deletion eliminating 1 amino acid from the LYST WD40 motif.[17] In addition to systemic defects resembling Chediak-Higashi syndrome,[35] B6-*Lyst$^{bg\text{-}J}$* mice exhibit iris defects resembling exfoliation syndrome.[17] The iris of B6-*Lyst$^{bg\text{-}J}$* mice undergoes an early-onset degenerative disease characterized by stromal atrophy, changes in the morphology of the iris pigment epithelium, and accumulation of pigment-engulfed macrophages.[17,20] As recently proposed in humans,[36] *Lyst* also influences iris color, resulting in dark-appearing irides.[19] Histologic indices of disease are absent in B6-*Lyst$^{bg\text{-}J}$* mice at 17 days of age, but are pronounced by 100 days of age.[20] Thus, at 60 days of age, the B6-*Lyst$^{bg\text{-}J}$* iris is in an active disease state characterized in slit lamp examination by a dark and granular-appearing iris with distinct transillumination defects (Figs. 2G–L). To identify transcriptional differences related to these exfoliative-like eyes, microarray analysis was performed on RNA isolated from the iris of 60-day-old B6-*Lyst$^{bg\text{-}J}$* mice.

The pair-wise comparison of RMA-normalized expression values between C57BL/6J and B6-*Lyst$^{bg\text{-}J}$* irides identified 460 transcripts with >1.8-fold changes in expression (262 overrepresented and 198 underrepresented). Among the transcripts with the largest change in expression (Table 1), the most striking observation was that several transcripts overrepresented in exfoliative-like irides were linked to immune responses. The most overrepresented transcripts were *Mmp12* (+56.8-fold), *Fabp4* (+44.4-fold), and *Atp6v0d2* (+43.2-fold). The most underrepre-

TABLE 3. Overrepresented Transcripts in B6.*Tyr*$^{c\text{-}2J}$ Irides

Gene Symbol	Gene Name	Change Ratio
Structural Constituent of Eye Lens		
Cryaa	Crystallin, alpha a	6.9
Cryba1	Crystallin, beta a1	3.5
Crybb2	Crystallin, beta b2	7.1
Cryga	Crystallin, gamma a	11.7
Cryab	Crystallin, alpha b	5.8
Visual Perception		
Guca1a	Guanylate cyclase activator 1a (retina)	2.8
Rcvrn	Recoverin	2.4
Rho	Rhodopsin	3.6
Rpe65	Retinal pigment epithelium 65	4.8
Rom1	Rod outer segment membrane protein 1	2.6
Cell Adhesion		
Cdh4	Cadherin 4	2.0
Cdh2	Cadherin 2	2.0
Cdh1	Cadherin 1	2.2
Ctnna2	Catenin (cadherin associated protein), alpha 2	2.1
Pcdh21	Protocadherin 21	2.9
Morphogenesis of an Epithelium		
Aldh1a1	Aldehyde dehydrogenase family 1, a1	2.7
Lama1	Laminin, alpha 1	2.8
Crygs	Crystallin, gamma s	4.6
Frem2	Fras1 related extracellular matrix protein 2	3.2
Pcdh8	Protocadherin 8	2.5
Pigmentation		
Sox2	Sry-box containing gene 2	8.5
Alad	Aminolevulinate, delta-, dehydratase	2.7
Immune System Process		
Spna1	Spectrin alpha 1	3.6
Itga6	Integrin alpha 6	2.4
Scg2	Secretogranin ii	3.4
Snap91	Synaptosomal-associated protein 91	1.9
Med1	Peroxisome proliferator activated receptor binding protein	1.8
Neurogenesis		
Timp2	Tissue inhibitor of metalloproteinase 2	1.9
Dner	Delta/notch-like egf-related receptor	4.0
Ntn4	Netrin 4	1.8
Stmn1	Stathmin 1	2.5
Nefl	Neurofilament, light polypeptide	7.0
Cell Death		
Bcl2l13	Bcl2-like 13 (apoptosis facilitator)	2.9
Fgfr3	Fibroblast growth factor receptor 3	4.1
Cntf	Ciliary neurotrophic factor	2.0
Brca1	Breast cancer 1	2.4
Dad1	Defender against cell death 1	1.8

All changes relative to irides of age- and sex-matched C57BL/6J mice.

TABLE 4. Underrepresented Transcripts in B6.*Tyr*$^{c\text{-}2J}$ Irides

Gene Symbol	Gene Name	Change Ratio
Enzyme linked Receptor Protein Signaling Pathway		
Ptprk	Protein tyrosine phosphatase, receptor type, k	−1.8
Gdnf	Glial cell line derived neurotrophic factor	−2.2
Met	Met proto-oncogene	−2.0
Figf	C-fos induced growth factor	−1.9
Flt1	FMS-like tyrosine kinase 1	−1.8
Extracellular Space		
Scrg1	Scrapie responsive gene 1	−2.0
Calcrl	Calcitonin receptor-like	−1.8
Ptn	Pleiotrophin	−1.9
Cxcl11	Chemokine (c-x-c motif) ligand 11	−1.9
Prss22	Protease, serine, 22	−2.0
Catalytic Activity		
Mpa2l	Macrophage activation 2 like	−2.0
Kcnh3	Potassium voltage-gated channel, subfamily h (EAG-related), member 3	−1.8
Mettl7a1	Methyltransferase like 7a	−2.1
Ugcg	UDP-glucose ceramide glucosyltransferase	−2.2
Ifih1	Interferon induced with helicase c domain 1	−2.0
Posttranslational Protein Modification		
Mmp14	Matrix metallopeptidase 14	−2.2
Bhmt	Betaine-homocysteine methyltransferase	−3.1
Rapgef3	Rap guanine nucleotide exchange factor 3	−2.5
Rapgef4	Rap guanine nucleotide exchange factor 4	−1.9
Camk2g	Calcium/calmodulin-dependent protein kinase II gamma	−1.8
Pigmentation		
Gpnmb	Glycoprotein (transmembrane) nmb	−2.1
Immune System Process		
Scin	Scinderin	−3.1
Cd8a	Cd8 antigen, alpha chain	−1.9
Mpa2l	Macrophage activation 2 like	−2.0
Tgtp	T-cell-specific GTPase	−2.2
Clec4d	C-type lectin domain family 4, member d	−2.3
Neurogenesis		
Zfhx3	AT motif binding factor 1	−2.3
Plp1	Proteolipid protein (myelin) 1	−1.8
Mtap1b	Microtubule-associated protein 1 b	−2.8
Cck	Cholecystokinin	−3.2
Notch3	Notch gene homolog 3	−1.9
Cell Death		
Tnfrsf11b	Tumor necrosis factor receptor superfamily, member 11b (osteoprotegerin)	−1.8
Gdnf	Glial cell line derived neurotrophic factor	−2.2
Aldh1a3	Aldehyde dehydrogenase family 1, subfamily a3	−2.1
Erbb3	V-erb-b2 erythroblastic leukemia viral oncogene homolog 3 (avian)	−2.1
Lyz2	Lysozyme	−1.9

All changes relative to irides of age- and sex-matched C57BL/6J mice.

TABLE 5. Overrepresented Transcripts in B6.*Tyrp1*^{b} *Gpnmb*^{R150X} Irides

Gene Symbol	Gene Name	Change Ratio
Structural Constituent of Eye Lens		
Cryaa	Crystallin, alpha a	5.1
Cryba1	Crystallin, beta a1	2.9
Crybb2	Crystallin, beta b2	5.2
Cryga	Crystallin, gamma a	5.1
Cryab	Crystallin, alpha b	4.6
Structural Molecule Activity		
Col4a2	Procollagen, type iv, alpha 2	3.7
Krt19	Keratin complex 1, acidic, gene 19	3.9
Ppl	Periplakin	1.8
Gfap	Glial fibrillary acidic protein	3.5
Lama1	Laminin, alpha 1	2.4
Organelle Inner Membrane		
Uqcr	Ubiquinol-cytochrome c reductase subunit	1.9
Cpxm1	Carboxypeptidase x 1 (m14 family)	2.3
Tst	Thiosulfate sulfurtransferase, mitochondrial	2.4
Hmgcs2	Hydroxymethylglutaryl-coa synthase 2	3.4
Ndufb7	Nadh dehydrogenase 1 beta subcomplex, 7	1.9
Morphogenesis of an Epithelium		
Aldh1a1	Aldehyde dehydrogenase family 1, a1	2.4
Car2	Carbonic anhydrase 2	2.3
Crygs	Crystallin, gamma s	3.4
Frem2	Fras1 related extracellular matrix protein 2	2.9
Fgfr3	Fibroblast growth factor receptor 3	3.0
Pigmentation		
Sox2	SRY-box containing gene 2	5.5
Alad	Aminolevulinate, delta-, dehydratase	2.6
Calm1	Calmodulin 1	1.9
Wnt7a	Wingless-related MMTV integration site 7a	2.2
Wnt7b	Wingless-related MMTV integration site 7b	4.1
Immune System Process		
Spon2	Spondin 2, extracellular matrix protein	4.4
C1qb	Complement component 1, q subcomponent, beta polypeptide	1.9
Spna1	Spectrin alpha 1	2.7
Cd24a	Cd24a antigen	6.3
Itga6	Integrin alpha 6	2.3
Neurogenesis		
Stmn1	Stathmin 1	2.7
Nefl	Neurofilament, light polypeptide	2.4
Hes5	Hairy and enhancer of split 5 (drosophila)	2.0
Cntf	Ciliary neurotrophic factor	1.8
Cck	Cholecystokinin	2.5
Cell Death		
Inhba	Inhibin beta-a	3.4
Msx1	Homeobox, MSH-like 1	2.1
Cdh1	Cadherin 1	1.9
Bcl2l13	Bcl2-like 13 (apoptosis facilitator)	2.6
Aplp1	Amyloid beta (a4) precursor-like protein 1	2.0

All changes relative to irides of age- and sex-matched C57BL/6J mice.

TABLE 6. Underrepresented Transcripts in B6.*Tyrp1*^{b} *Gpnmb*^{R150X} *Irides*

Gene Symbol	Gene Name	Change Ratio
Anatomical Structure Development		
Myom2	Myomesin 2	−2.3
Met	Met proto-oncogene	−1.9
Ing3	Inhibitor of growth family, member 3	−3.3
Otor	Otoraplin	−2.1
Ugcg	UDP-glucose ceramide glucosyltransferase	−1.9
Negative Regulation of Cellular Process		
Rgs7bp	Regulator of G-protein signaling 7-binding protein	−2.1
Spnb2	Spectrin beta 2	−1.9
Cav2	Caveolin 2	−1.8
Nlk	Nemo-like kinase	−2.4
Taok3	Tao kinase 3	−2.7
Regulation of Transcription		
Sox11	SRY-box containing gene 11	−2.5
Elk4	Elk4, member of ETS oncogene family	−2.6
Plcb4	Phospholipase c, beta 4	−2.0
Zeb2	Zinc finger homeobox 1b	−1.8
Ebf1	Early b-cell factor 1	−1.9
Posttranslational Protein Modification		
Ptprd	Protein tyrosine phosphatase, receptor type, d	−2.2
Pja2	Praja 2, ring-h2 motif containing	−2.7
Art3	ADP-ribosyltransferase 3	−1.9
Ttn	Titin	−1.9
Rapgef4	Rap guanine nucleotide exchange factor 4	−1.8
Pigmentation		
Rab27a	Rab27a, member ras oncogene family	−1.8
Gpnmb	Glycoprotein (transmembrane) nmb	−9.4
Immune System Process		
Cd274	Cd274 antigen	−1.8
Pdk1	Pyruvate dehydrogenase kinase, isoenzyme 1	−2.1
Neurogenesis		
Zfhx3	At motif binding factor 1	−2.4
Gpr124	G protein-coupled receptor 124	−2.1
Vapb	Vamp-associated protein 33b	−2.1
Mtap1b	Microtubule-associated protein 1 b	−2.8
Eml2	Echinoderm microtubule associated protein like 2	−1.9
Cell Death		
Cul4a	Cullin 4a	−2.2
Sgms1	Sphingomyelin synthase 1	−2.7
Bcl2	B-cell leukemia/lymphoma 2	−1.8

All changes relative to irides of age- and sex-matched C57BL/6J mice.

TABLE 7. Overrepresented Transcripts in B6-*Lyst*$^{bg\text{-}J}$ Irides

Gene Symbol	Gene Name	Change Ratio
Cell Adhesion		
Itgax	Integrin alpha x	16.6
Itgb3	Integrin beta 3	4.9
Itgb2	Integrin beta 2	20.0
Fblim1	Filamin binding lim protein 1	2.2
Parvg	Parvin, gamma	1.8
Lysosome		
Ctsd	Cathepsin d	2.4
Ctsb	Cathepsin b	2.2
Lipa	Lysosomal acid lipase 1	2.9
Npc2	Niemann pick type c2	1.8
Laptm5	Lysosomal-associated protein transmembrane 5	6.0
Inflammatory Response		
Tlr13	Toll-like receptor 13	6.3
Pparg	Peroxisome proliferator activated receptor gamma	2.2
Pla2g7	Phospholipase a2, group vii	3.0
Ncf1	Neutrophil cytosolic factor 1	2.5
Ly86	Lymphocyte antigen 86	2.8
Phagocytosis		
Clec7a	C-type lectin domain family 7, member a	15.5
Sirpb1	Sirp-beta b	3.5
Fcgr3	Fc receptor, IGG, low affinity iii	6.0
Mfge8	Milk fat globule-egf factor 8 protein	4.3
Fcer1g	Fc receptor, IGE, high affinity I, gamma polypeptide	4.0
Pigmentation		
Calm1	Calmodulin 1	2.1
Adcy7	Adenylate cyclase 7	3.4
Immune System Process		
C3ar1	Complement component 3a receptor 1	8.2
C1qa	Complement component 1, q subcomponent, alpha polypeptide	1.8
Scap2	SRC family associated phosphoprotein 2	2.0
Il1rl1	Interleukin 1 receptor-like 1	2.4
Irf8	Interferon regulatory factor 8	3.8
Neurogenesis		
Emr1	EGF-like module containing, mucin-like, hormone receptor-like sequence 1	3.3
Erg2	Early growth response 2	4.6
Cdkn1c	Cyclin-dependent kinase inhibitor 1c (p57)	3.2
Sema4d	Semaphorin 4D	2.1
Alcam	Activated leukocyte cell adhesion molecule	2.1
Cell Death		
Casp1	Caspase 1	3.6
Naip5	NLR family, apoptosis inhibitory protein 5	3.6
Tnfrsf1b	Tumor necrosis factor receptor superfamily, member 1b	2.9
Bid	Bh3 interacting domain death agonist	1.8
Lyz2	Lysozyme	14.6

All changes relative to irides of age- and sex-matched C57BL/6J mice.

TABLE 8. Underrepresented Transcripts in B6-*Lyst*$^{bg\text{-}J}$ Irides

Gene Symbol	Gene Name	Change Ratio
Extracellular Matrix		
Fmod	Fibromodulin	−1.9
Ltbp3	Latent transforming growth factor beta binding protein 3	−2.0
Ltbp1	Latent transforming growth factor beta binding protein 1	−2.6
Frem1	Fras1 related extracellular matrix protein 1	−2.9
Utrn	Utrophin	−2.0
Cell Adhesion		
Cldn1	Claudin 1	−2.6
Cntn1	Contactin 1	−1.8
Muc4	Mucin 4	−3.3
Mpzl2	Epithelial v-like antigen 1	−2.3
Thbs1	Thrombospondin 1	−2.1
Ion Transport		
Best2	Bestrophin 2	−2.0
Trpm1	Transient receptor potential cation channel, subfamily m, member 1	−2.0
Clic6	Chloride intracellular channel 6	−2.3
Stim1	Stromal interaction molecule 1	−1.9
Slc12a6	Solute carrier family 12, member 6	−2.3
Structural Constituent of Cytoskeleton		
Krt12	Keratin complex 1, acidic, gene 12	−6.1
Krt6a	Keratin complex 2, basic, gene 6a	−3.7
Krt5	Keratin 5	−3.8
Ttn	Titin	−1.8
Myom2	Myomesin 2	−2.3
Pigmentation		
Gsk3b	Glycogen synthase kinase 3 beta	−2.0
Immune System Process		
Sp3	Trans-acting transcription factor 3	−1.9
Defb1	Defensin beta 1	−2.0
Zbtb16	Zinc finger and BTB domain containing 16	−2.0
Ndrg1	N-myc downstream regulated gene 1	−1.8
Neurogenesis		
Cck	Cholecystokinin	−2.9
Id4	Inhibitor of DNA binding 4	−2.0
Erbb3	V-erb-b2 erythroblastic leukemia viral oncogene homolog 3 (avian)	−1.9
Mtap1b	Microtubule-associated protein 1 b	−3.0
Slit2	Slit homolog 2 (drosophila)	−2.2
Cell Death		
Son	Son cell proliferation protein	−1.9
Eya1	Eyes absent 1 homolog (drosophila)	−2.0
Sgpp1	Sphingosine-1-phosphate phosphatase 1	−1.9
1810011O10Rik	Riken cDNA 1810011o10 gene	−2.0
A330102K23Rik	Riken cDNA a330102k23 gene	−2.2

All changes relative to irides of age- and sex-matched C57BL/6J mice.

sented transcripts were *Prpmp5* (−8.7-fold), *Krt12* (−6.1-fold), and *Tmprss11e* (−4.0-fold). Exfoliative-like irides also exhibited expression changes in several groups of genes of biological interest (Tables 7, 8), including changes in the expression of several genes associated with lytic vacuoles and lysosomes. Changes in *Lyst* expression were not detected.

Validation Using Quantitative Real-Time PCR

To validate the expression changes obtained from microarray analyses, a subset of transcripts were independently tested with qRT-PCR. In a separate cohort of mice, examples of overrepresented and underrepresented transcripts were confirmed in the analysis of B6.*Tyr*$^{c\text{-}2J}$ (*Gja3*, +14.9-fold; *B3Gnt5*, +123.0-fold; *Cryba4*, +86,951-fold; *Muc 4*, −2.9-fold; *Myom2*, −14.2-fold; and *Gpnmb*, −5.32-fold), B6.*Tyrp1*^{b} *Gpnmb*^{R150X} (*Gja3*, +10.1-fold; *B3gnt5*, +23.0-fold; and *Gpnmb*, -7.3-fold), and B6-*Lyst*$^{bg\text{-}J}$ irides (*Mmp12*, +231.2-fold; *Ltbp1*, −5.4-fold; and *Ltbp2*, −28.9-fold). Transcripts of several genes relevant to ocular disease, but not predicted to be differentially expressed by the microarray analysis, were also analyzed by qRT-PCR and were confirmed not to be differentially expressed (*Tyr*, *Cyp1b1*, *Edn3*, *Foxc1*, and *Mitf*; <1.8-fold changes in all comparisons to C57BL/6J).

Discussion

We investigated genome-wide iridial transcriptional profiles of wild-type C57BL/6J mice and three strains with iridial diseases, one modeling OCA (B6.*Tyr*$^{c\text{-}2J}$), one modeling pigment dispersion syndrome (B6.*Tyrp1*^{b} *Gpnmb*^{R150X}), and one modeling exfoliation syndrome (B6-*Lyst*$^{bg\text{-}J}$). The mutations of these strains are also all relevant to glaucoma. In comparisons between each genetic context, a large number of expression changes were detected. These findings have several biologically relevant implications and represent a useful resource as a hypothesis-generating dataset.

With respect to OCA, perhaps the most surprising observation was the large number of changing transcripts associated with tyrosinase mutation. Among the strains analyzed, the greatest number of differentially expressed transcripts was observed in the comparison of albino versus normally pigmented C57BL/6J mice (685 transcripts with >1.8-fold changes in expression). Surprisingly, a substantial pigment-related gene ontology signal was not detected. The overrepresented transcripts related to visual perception were initially unexpected, although there are other reports of genes such as rhodopsin being expressed in the iris.[37] Among the transcripts related to structural elements of the lens, several were crystallins, which have also been found to be expressed in the human iris.[38] In addition to being a main structural element of the lens, crystallins have been proposed to function outside of the lens as chaperones active in responses to damaging stimuli such as oxidative stress.[39] As discussed below, the changes in crystallin gene expression detected in this study overlap a genetic network of crystallin genes previously observed to be coexpressed in mouse retina and brain, as well.[40] Further studies would be needed to stringently discern whether the visual perception or structural elements of the lens signals detected are biological or a consequence of trace contamination from the retina and lens, which is certainly possible.[41] However, changes in prevalent non-crystallin–related lens transcripts (such as *Gluld1*) or other prevalent retinal transcripts (such as *Prph2*) were not detected, suggesting that the changes observed are biological.

Several observations were made relevant to pigment dispersion and glaucoma. First, a locus involved in hereditary pigment dispersion syndrome in humans has been proposed at 7q35-q36,[9] but causative mutations have not yet been identified. Three genes identified in our microarray analysis of pigment dispersion–prone mice are located within the regions of conserved synteny in mice (*A230106D06Rik*, −2.2-fold; *Kcnb2*, +2.6-fold; and *Crygn*, +5.4-fold). Therefore, each of these is worthy of consideration as a candidate for involvement in human disease. Second, there are many similarities between the transcriptional changes detected in the iris of B6.*Tyrp1*^{b} *Gpnmb*^{R150X} mice and those previously observed in the retina of DBA/2J mice.[42] Notably, of the 36 downregulated transcripts detected in the retina of 8-month-old versus 3-month-old DBA/2J mice,[42] 14 were also detected in our analysis of the iris in 60-day-old B6.*Tyrp1*^{b} *Gpnmb*^{R150X} mice. Indeed, 10 of these changes were among the top 25 overrepresented transcripts in B6.*Tyrp1*^{b} *Gpnmb*^{R150X} mice (*Cryba2*, *Cryba4*, *Cd24a*, *Crybb3*, *Grifin*, *Crygb*, *Crybb1*, *Crygd*, *Crygn*, *Cryaa*, and *Adamsts18*). The direction of the changes among these overlapping signals is in opposing directions, being overrepresented in the pre-disease-state iris of 60-day-old B6.*Tyrp1*^{b} *Gpnmb*^{R150X} mice and underrepresented in the active disease state retina of 8-month-old DBA/2J mice. Though speculative, this relationship may indicate a crystallin-mediated stress response active in the iris and retina of young mice, which falters as glaucoma ensues. Overlaps with findings of Panagis et al.,[43] who studied expression changes in damaged areas of individual glaucomatous DBA/2J retinas versus undamaged areas, were less striking. Of the top 30 upregulated and downregulated transcripts identified by Panagis et al., only 1 was also altered in the iris of B6.*Tyrp1*^{b} *Gpnmb*^{R150X} mice (*9430051O21Rik*, −1.8-fold). With respect to pigmentary glaucoma, it is noteworthy that 1 gene, *Crygn*, is located at chromosomal position 7q35–36 in humans, has altered expression in the iris of pigment dispersion–prone mice (+5.4-fold), and has altered expression in the retina of glaucomatous DBA/2J mice (−2.3-fold).[42]

In irides of exfoliative-like B6-*Lyst*$^{bg\text{-}J}$ mice, the transcript with the overall largest ratio of change in expression compared with C57BL/6J control irides was *Mmp12* (+56.8-fold in microarray, +231.2-fold in qRT-PCR). MMP12 belongs to a family of structurally related extracellular matrix–degrading enzymes that are collectively capable of degrading essentially all extracellular matrix components.[44] MMP12 has several substrates, notably including elastin.[45] In most tissues, MMP12 is mainly produced by macrophages,[46] although in ocular tissues it has also been found in cultured trabecular meshwork cells[47] and cultured keratocytes.[48] *Mmp12* expression is upregulated by TGF-β.[49] Because exfoliation syndrome involves changes in both TGF-β and elastin,[15] this dramatic expression difference observed in a mouse model suggests that MMP12 makes direct contributions to disease phenotypes that occur in exfoliation syndrome. Using mice with genetic perturbations in *Mmp12*, we are currently testing this hypothesis directly.

Among the molecular signatures identified from comparisons of the four strains studied, one of the most striking observations was that albino and pigment dispersion–prone irides both exhibited evidence of a crystallin-mediated stress response. In a recent study of differential responses of C57BL/6J and DBA/2J mice to optic nerve crush, Templeton et al.[40] identified a very similar response from a genetic network of co-regulated crystallin genes downregulated in the C57BL/6J retina and upregulated in the DBA/2J retina at 2 days after optic nerve crush. Of the 12 members of this family (*Cryaa*, *Cryab*, *Cryba1*, *Cryba2*, *Cryba4*, *Crybb1*, *Crybb2*, *Crybb3*, *Crygb*, *Crygc*, *Crygd*, and *Crygs*), all 12 were overrepresented in the iris of albino B6.*Tyr*$^{c\text{-}2J}$ mice compared with wild-type C57BL/6J and 11 were overrepresented in the iris of pigment dispersion–prone B6.*Tyrp1*^{b} *Gpnmb*^{R150X} mice compared with wild-type C57BL/6J (changes in *Crgd* were not detected). The same co-regulatory network has also been detected in the

hippocampus of mice, absolutely ruling out the possibility that this signature is a simple consequence of lens contamination.[40] Rather, it appears that across many different tissues, a wide variety of stresses can induce co-expression of this genetic network.

Although the current experimental design allowed identification of many changes, it also had caveats. One limitation of our present study is that we used a mouse model of pigment dispersion syndrome harboring mutations in both *Tyrp1* and *Gpnmb*. Thus, it is not possible to differentiate which expression changes were caused by *Tyrp1* mutation by itself, *Gpnmb* mutation by itself, or their combined interaction. Another important factor of the present study design is that individual iris cell types were not separated. Although the iris is one of the body's most concentrated sources of pigmented cells and their signature is likely a predominant one, the iris does have a variety of other cell types. The mouse iris stroma primarily consists of melanocytes derived from the periocular mesenchyme, small blood vessels, and antigen-presenting cells; the iris pigment epithelium consists of two pigmented neural epithelium–derived cell layers, the anterior of which is the source of both the iris sphincter and dilator smooth muscles.[50–55] Thus, for changing transcripts such as *Gpnmb* (underrepresented in albino and pigment dispersion–prone irides), which is known to be expressed in pigmented cells and antigen presenting cells,[28,56] it is not clear which cells give rise to the signal detected in the current microarray study of the entire iris. Finally, the present study did not follow temporal changes in gene expression. Although the 60-day-old time point represents a time when disease phenotypes are readily apparent by slit lamp examination in albino and exfoliative-like mice,[17,19] it is a time when iris disease is not yet clinically detectable for pigment dispersion–prone mice.[5]

In summary, we used genome-wide microarray analysis to study iris samples of wild-type C57BL/6J mice, albino mice with a *Tyr* mutation, pigment dispersion–prone mice with *Tyrp1* and *Gpnmb* mutations, and mice resembling exfoliation syndrome with a *Lyst* mutation. In comparisons between each genetic context, a large number of expression changes were detected. The results identify many candidate genes that may be active in these diseases and represent a useful resource for further mechanistic studies.

Acknowledgments

The authors thank Greg Petersen and Adam Hedberg-Buenz for help maintaining mouse colonies; Trish Duffel for assistance in preparing the tables; and Kevin Knudtson (University of Iowa DNA Facility) for technical assistance with the microarrays.

References

1. Gronskov K, Ek J, Brondum-Nielsen K. Oculocutaneous albinism. *Orphanet J Rare Dis.* 2007;2:43.
2. Hutton SM, Spritz RA. Comprehensive analysis of oculocutaneous albinism among non-Hispanic caucasians shows that OCA1 is the most prevalent OCA type. *J Invest Dermatol.* 2008;128:2442–2450.
3. Oetting WS, Fryer JP, Shriram S, King RA. Oculocutaneous albinism type 1: the last 100 years. *Pigment Cell Res.* 2003;16:307–311.
4. Ray K, Chaki M, Sengupta M. Tyrosinase and ocular diseases: some novel thoughts on the molecular basis of oculocutaneous albinism type 1. *Prog Retin Eye Res.* 2007;26:323–358.
5. Anderson MG, Libby RT, Mao M, et al. Genetic context determines susceptibility to intraocular pressure elevation in a mouse pigmentary glaucoma. *BMC Biol.* 2006;4:20.
6. Libby RT, Smith RS, Savinova OV, et al. Modification of ocular defects in mouse developmental glaucoma models by tyrosinase. *Science.* 2003;299:1578–1581.
7. Ball SF. Pigmentary glaucoma. In: Yanoff M, Duker JS, ed. *Ophthalmology*. St Louis: Mosby; 2004;1504–1507.
8. Ritch R. A unification hypothesis of pigment dispersion syndrome. *Trans Am Ophthalmol Soc.* 1996;94:381–405, discussion 405–389.
9. Andersen JS, Pralea AM, DelBono EA, et al. A gene responsible for the pigment dispersion syndrome maps to chromosome 7q35–q36. *Arch Ophthalmol.* 1997;115:384–388.
10. Mandelkorn RM, Hoffman ME, Olander KW, Zimmerman T, Harsha D. Inheritance and the pigmentary dispersion syndrome. *Ann Ophthalmol.* 1983;15:577–582.
11. John SW, Smith RS, Savinova OV, et al. Essential iris atrophy, pigment dispersion, and glaucoma in DBA/2J mice. *Invest Ophthalmol Vis Sci.* 1998;39:951–962.
12. Libby RT, Anderson MG, Pang IH, et al. Inherited glaucoma in DBA/2J mice: pertinent disease features for studying the neurodegeneration. *Vis Neurosci.* 2005;22:637–648.
13. Anderson MG, Smith RS, Hawes NL, et al. Mutations in genes encoding melanosomal proteins cause pigmentary glaucoma in DBA/2J mice. *Nat Genet.* 2002;30:81–85.
14. Lynch S, Yanagi G, DelBono E, Wiggs JL. DNA sequence variants in the tyrosinase-related protein 1 (TYRP1) gene are not associated with human pigmentary glaucoma. *Mol Vis.* 2002;8:127–129.
15. Schlotzer-Schrehardt U, Naumann GO. Ocular and systemic pseudoexfoliation syndrome. *Am J Ophthalmol.* 2006;141:921–937.
16. Hammer T, Schlotzer-Schrehardt U, Naumann GO. Unilateral or asymmetric pseudoexfoliation syndrome?—an ultrastructural study. *Arch Ophthalmol.* 2001;119:1023–1031.
17. Trantow CM, Mao M, Petersen GE, et al. Lyst mutation in mice recapitulates iris defects of human exfoliation syndrome. *Invest Ophthalmol Vis Sci.* 2009;50:1205–1214.
18. Thorleifsson G, Magnusson KP, Sulem P, et al. Common sequence variants in the LOXL1 gene confer susceptibility to exfoliation glaucoma. *Science.* 2007;317:1397–1400.
19. Anderson MG, Hawes NL, Trantow CM, Chang B, John SW. Iris phenotypes and pigment dispersion caused by genes influencing pigmentation. *Pigment Cell Melanoma Res.* 2008;21:565–578.
20. Trantow CM, Hedberg-Buenz A, Iwashita S, Moore SA, Anderson MG. Elevated oxidative membrane damage associated with genetic modifiers of lyst-mutant phenotypes. *PLoS Genet.* 2010;6:e1001008.
21. Irizarry RA, Bolstad BM, Collin F, Cope LM, Hobbs B, Speed TP. Summaries of Affymetrix GeneChip probe level data. *Nucleic Acids Res.* 2003;31:e15.
22. Tusher VG, Tibshirani R, Chu G. Significance analysis of microarrays applied to the ionizing radiation response. *Proc Natl Acad Sci U S A.* 2001;98:5116–5121.
23. Dennis G, Jr., Sherman BT, Hosack DA, et al. DAVID: Database For Annotation, Visualization, and Integrated Discovery. *Genome Biol.* 2003;4:P3.
24. Huang da W, Sherman BT, Lempicki RA. Systematic and integrative analysis of large gene lists using DAVID Bioinformatics Resources. *Nat Protoc.* 2009;4:44–57.
25. Pfaffl MW. A new mathematical model for relative quantification in real-time RT-PCR. *Nucleic Acids Res.* 2001;29:e45.
26. Le Fur N, Kelsall SR, Mintz B. Base substitution at different alternative splice donor sites of the tyrosinase gene in murine albinism. *Genomics.* 1996;37:245–248.
27. Zdarsky E, Favor J, Jackson IJ. The molecular basis of brown, an old mouse mutation, and of an induced revertant to wild type. *Genetics.* 1990;126:443–449.
28. Anderson MG, Nair KS, Amonoo LA, et al. GpnmbR150X allele must be present in bone marrow derived cells to mediate DBA/2J glaucoma. *BMC Genet.* 2008;9:30.
29. Schraermeyer M, Schnichels S, Julien S, Heiduschka P, Bartz-Schmidt KU, Schraermeyer U. Ultrastructural analysis of the pigment dispersion syndrome in DBA/2J mice. *Graefes Arch Clin Exp Ophthalmol.* 2009;247:1493–1504.
30. Mo JS, Anderson MG, Gregory M, et al. By altering ocular immune privilege, bone marrow-derived cells pathogenically contribute to DBA/2J pigmentary glaucoma. *J Exp Med.* 2003;197:1335–1344.

31. Kuehn MH, Kim CY, Ostojic J, et al. Retinal synthesis and deposition of complement components induced by ocular hypertension. *Exp Eye Res.* 2006;83:620–628.
32. Nickells RW, Semaan SJ, Schlamp CL. Involvement of the Bcl2 gene family in the signaling and control of retinal ganglion cell death. *Prog Brain Res.* 2008;173:423–435.
33. Pease ME, Zack DJ, Berlinicke C, et al. Effect of CNTF on retinal ganglion cell survival in experimental glaucoma. *Invest Ophthalmol Vis Sci.* 2009;50:2194–2200.
34. Kaplan J, De Domenico I, Ward DM. Chediak-Higashi syndrome. *Curr Opin Hematol.* 2008;15:22–29.
35. Barbosa MD, Nguyen QA, Tchernev VT, et al. Identification of the homologous beige and Chediak-Higashi syndrome genes. *Nature.* 1996;382:262–265.
36. Liu F, Wollstein A, Hysi PG, et al. Digital quantification of human eye color highlights genetic association of three new loci. *PLoS Genet.* 2010;6:e1000934.
37. Ghosh S, Salvador-Silva M, Coca-Prados M. The bovine iris-ciliary epithelium expresses components of rod phototransduction. *Neurosci Lett.* 2004;370:7–12.
38. Friedman JS, Koop BF, Raymond V, Walter MA. Isolation of a ubiquitin-like (UBL5) gene from a screen identifying highly expressed and conserved iris genes. *Genomics.* 2001;71:252–255.
39. Graw J. Genetics of crystallins: cataract and beyond. *Exp Eye Res.* 2009;88:173–189.
40. Templeton JP, Nassr M, Vazquez-Chona F, et al. Differential response of C57BL/6J mouse and DBA/2J mouse to optic nerve crush. *BMC Neurosci.* 2009;10:90.
41. Kamphuis W, Dijk F, Kraan W, Bergen AA. Transfer of lens-specific transcripts to retinal RNA samples may underlie observed changes in crystallin-gene transcript levels after ischemia. *Mol Vis.* 2007;13:220–228.
42. Steele MR, Inman DM, Calkins DJ, Horner PJ, Vetter ML. Microarray analysis of retinal gene expression in the DBA/2J model of glaucoma. *Invest Ophthalmol Vis Sci.* 2006;47:977–985.
43. Panagis L, Zhao X, Ge Y, Ren L, Mittag TW, Danias J. Gene expression changes in areas of focal loss of retinal ganglion cells (RGC) in the retina of DBA/2J Mice. *Invest Ophthalmol Vis Sci.* 2010;51:2024–2034.
44. Brinckerhoff CE, Matrisian LM. Matrix metalloproteinases: a tail of a frog that became a prince. *Nat Rev Mol Cell Biol.* 2002;3:207–214.
45. Gronski TJ Jr, Martin RL, Kobayashi DK, et al. Hydrolysis of a broad spectrum of extracellular matrix proteins by human macrophage elastase. *J Biol Chem.* 1997;272:12189–12194.
46. Nenan S, Boichot E, Lagente V, Bertrand CP. Macrophage elastase (MMP-12): a pro-inflammatory mediator? *Mem Inst Oswaldo Cruz.* 2005;100(Suppl 1):167–172.
47. Kelley MJ, Rose AY, Song K, et al. Synergism of TNF and IL-1 in the induction of matrix metalloproteinase-3 in trabecular meshwork. *Invest Ophthalmol Vis Sci.* 2007;48:2634–2643.
48. Chakravarti S, Wu F, Vij N, Roberts L, Joyce S. Microarray studies reveal macrophage-like function of stromal keratocytes in the cornea. *Invest Ophthalmol Vis Sci.* 2004;45:3475–3484.
49. Lagente V, Le Quement C, Boichot E. Macrophage metalloelastase (MMP-12) as a target for inflammatory respiratory diseases. *Expert Opin Ther Targets.* 2009;13:287–295.
50. Gage PJ, Rhoades W, Prucka SK, Hjalt T. Fate maps of neural crest and mesoderm in the mammalian eye. *Invest Ophthalmol Vis Sci.* 2005;46:4200–4208.
51. McMenamin PG, Crewe J, Morrison S, Holt PG. Immunomorphologic studies of macrophages and MHC class II-positive dendritic cells in the iris and ciliary body of the rat, mouse, and human eye. *Invest Ophthalmol Vis Sci.* 1994;35:3234–3250.
52. Smith RS, ed. *Systemic Evaluation of the Mouse Eye*. Boca Raton, FL: CRC Press LLC; 2002.
53. Yamashita T. Fine structure of the sphincter and dilator muscles of the pupil of the mouse. *Okajimas Folia Anat Jpn.* 1984;61:161–165.
54. Yamashita T, Takahashi A, Honjin R. Fine structure, origin, and distribution density of the autonomic nerve endings in the sphincter and dilator muscles of the pupil of the mouse. *Okajimas Folia Anat Jpn.* 1984;61:173–181.
55. Smith RS. Ultrastructural studies of the blood-aqueous barrier. I. Transport of an electron-dense tracer in the iris and ciliary body of the mouse. *Am J Ophthalmol.* 1971;71:1066–1077.
56. Shikano S, Bonkobara M, Zukas PK, Ariizumi K. Molecular cloning of a dendritic cell-associated transmembrane protein, DC-HIL, that promotes RGD-dependent adhesion of endothelial cells through recognition of heparan sulfate proteoglycans. *J Biol Chem.* 2001;276:8125–8134.